

MFM-Net: Unpaired Shape Completion Network with Multi-stage Feature Matching

Zhen Cao^{1*}, Wenxiao Zhang^{1*}, Xin Wen², Zhen Dong^{1†}, Yu-shen Liu³, Bisheng Yang¹

¹Wuhan University, ²JD.com, ³Tsinghua University

{zhen.cao, dongzhenwhu, bshyang}@whu.edu.cn, wenxxiao.zhang@gmail.com

wenxin16@jd.com, liuyushen@tsinghua.edu.cn

Abstract

Unpaired 3D object completion aims to predict a complete 3D shape from an incomplete input without knowing the correspondence between the complete and incomplete shapes during training. To build the correspondence between two data modalities, previous methods usually apply adversarial training to match the global shape features extracted by the encoder. However, this ignores the correspondence between multi-scaled geometric information embedded in the pyramidal hierarchy of the decoder, which makes previous methods struggle to generate high-quality complete shapes. To address this problem, we propose a novel unpaired shape completion network, named MFM-Net, using multi-stage feature matching, which decomposes the learning of geometric correspondence into multi-stages throughout the hierarchical generation process in the point cloud decoder. Specifically, MFM-Net adopts a dual path architecture to establish multiple feature matching channels in different layers of the decoder, which is then combined with the adversarial learning to merge the distribution of features from complete and incomplete modalities. In addition, a refinement is applied to enhance the details. As a result, MFM-Net makes use of a more comprehensive understanding to establish the geometric correspondence between complete and incomplete shapes in a local-to-global perspective, which enables more detailed geometric inference for generating high-quality complete shapes. We conduct comprehensive experiments on several datasets, and the results show that our method outperforms previous methods of unpaired point cloud completion with a large margin.

1. Introduction

Point clouds, as a popular representation form of 3D geometries, have drawn a growing research concern in many fields, such as computer vision [23, 24, 33], robotics [16],

and auto-navigation [46]. However, the raw point clouds obtained by 3D scanning devices are often sparse, noisy and incomplete, which requires preprocessing (e.g. completion, denoising) before the downstream task. In this paper, we focus on the specific task to predict the complete shape for an incomplete point cloud, where the missing shape is usually caused by the single-view scanning. The common practice of previous deep learning based completion methods [14, 17, 41, 45] is to train a deep neural network under the supervision of incomplete shape and its paired complete ground truth. Although methods along this line have achieved impressive progress in recent years, their performance is still limited by the insufficiency of paired training data. Because it is difficult to obtain the paired ground truth for incomplete shape in real-world scenarios, due to laborious scanning for every view-angle and corners of the 3D shape.

A promising solution to this problem is to train the completion network only through the unpaired supervision. That is, only the collections of incomplete shapes and complete shapes are given to the network, where no paired information is revealed to the network. The intuition behind this practice is that, it is easy to obtain incomplete scanning in real-world, and the complete shapes can be collected from many large-scaled 3D shape datasets [3, 21]. Therefore, two sources of 3D shape datasets provide abundant unpaired training data, which can be used to improve the performance and generalization ability of completion network.

Following the above-mentioned idea, previous unpaired completion methods [4, 34] usually fulfill the task by adopting an adversarial framework with auto-encoders, which aim to narrow down the gap between the incomplete shapes and the complete ground truths. The problem is that, these methods mainly focus on the overall geometric correspondence between the incomplete shape and the complete shape, which is usually established by bridging the distribution gap between the global features of incomplete shapes and complete shapes. However, such practice ignores the

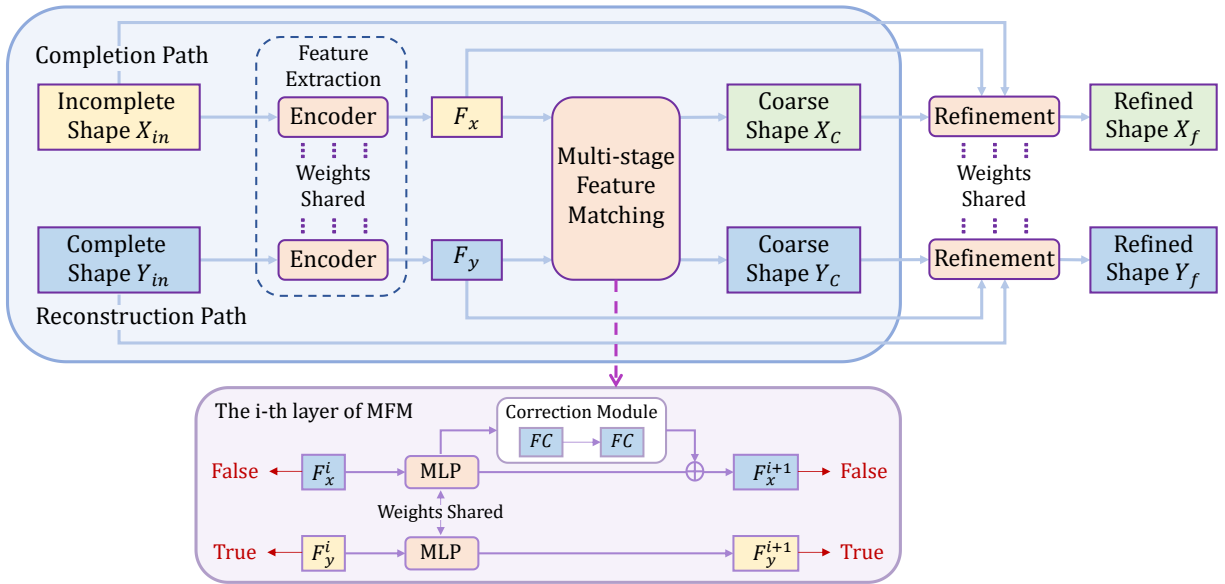


Figure 1. An illustration of our framework, which contains two different paths. The above is the completion path, which is used to convert an incomplete shape into a complete one, while the below is the reconstruction path, which is used to reconstruct the complete shape. We use Correction Module in the completion path, so that we can explicitly correct the features of this path to adapt to the task of point cloud completion.

abundant geometric information implicitly revealed by the generation process throughout the pyramidal hierarchy of the decoder, which can be further utilized to establish more detailed geometric correspondence between the complete shapes and incomplete shapes. In this paper, we address the importance of learning detailed geometric correspondence from the hierarchical structure of decoder, and significantly improve the performance of unpaired 3D shape completion.

Specifically, we propose a novel unpaired shape completion network, named MFM-Net, to decompose the learning of geometric correspondence into multi-stages along the hierarchical generation process of the point cloud decoder. Specifically, MFM-Net establishes multiple feature matching process at different layers of the decoder, which is then combined with the adversarial learning to merge the distribution of features from complete and incomplete domains. As shown in Fig. 1, in order to adapt to the multi-stage matching mechanism, we introduce a dual-path architecture, i.e., the reconstruction path of complete shape and the completion path of incomplete shape. Unlike Pcl2Pcl [4] and Cycle4Completion [34], which use two separate encoders, we adopt a shared-encoder to extract the features of the input point cloud, making the extracted features distribute more properly in the same latent space. As illustrated in Fig. 1, we embed both incomplete and complete point clouds via a weights shared encoder. And

then, we accomplish the feature transformation through a multi-stage matching process. Specifically, we involve a feature correction module to predict the residual features across these two paths in each stage, which thus progressively narrows the feature difference between incomplete and complete domains. As a result, MFM-Net can better explore the correspondence between complete and incomplete shapes through multiple matching process, thus performing more accurate geometric inference for high-quality complete shape generation.

In addition, the compact global feature cannot well capture detail information, thus the recovered complete shape from a global feature tends to lose local details. To this end, we develop a refinement module to reconstruct the results with enhanced local details. This module not only enhances the shape details but also involves global information to keep the shape smooth during the reconstruction.

Our main contributions are summarized as follows.

- We propose a novel unpaired shape completion network called MFM-Net and introduce a dual path framework to adapt to the unpaired shape completion task. Compared with the previous methods that only consider global feature matching, MFM-Net can enhance 3D shape understanding ability by building multiple feature matching process at different layers of the decoder, which leads to a better completion effect.

And the way that the two paths share most parameters is effective and economical, and can better capture geometric primitive features of similar local shapes.

- We develop a refinement module to enhance the details of the results. The refinement takes both local and global refinements into consideration, which can enhance the details while keeping the shape from distortion.
- We conduct comprehensive experiments on several datasets and show that our method can achieve SOTA performance over the previous unpaired point cloud completion methods.

2. Related Work

Traditional Shape Completion Methods. Traditional point cloud completion methods generally utilize the geometric attributes of objects [2, 6, 12, 18] or retrieval of the complete structure in the database [7, 9, 10, 15]. These methods usually leverage the artificially constructed features for completion, which cannot handle the cases with large missing parts.

3D Shape Completion with Pair Supervision. With the development of deep neural network, researchers tend to leverage learning-based methods for 3D shape completion. Early methods are based on the 3D voxel grid [5, 30, 42], but they are limited by the large computation which increases significantly with the increase of the shape resolution. Since PointNet [23] solved the disorder problem of point cloud, deep learning methods based on point cloud have been developed. PCN [45] is the first learning-based network that can directly operate on point clouds. PCN uses an encoder similar to PointNet to extract the global feature from the input point cloud directly, and then employs a decoder to infer the complete point cloud from the global feature. More recent works [1, 8, 11, 13, 14, 17, 25, 35, 38, 40, 44, 50] have made efforts to preserve the observed geometric details from the local features in incomplete inputs. NSFA [49] separately reconstruct the unknown and known parts. VRC-Net [21] proposes a variational framework by leveraging the relationship between structures during the completion process. PMP-Net [36] accomplish the completion task by learning point moving paths. Snowflakenet [39] propose a snowflake point deconvolution with skip-transformer for point cloud completion. There are also some networks using voxel-based completion process. GRNet [41] proposes a gridding network for dense point reconstruction. VE-PCN [31] develop a voxel-based network for point cloud completion by leveraging edge generation.

3D Shape Completion without Pair Supervision. On the other hand, there are few studies on unpaired shape completion. AML [27] uses the maximum likelihood method

to measure the distance between complete and incomplete point clouds in the latent space. Pcl2Pcl [4] pretrains two auto-encoders, and directly learns the mapping from partial shapes to the complete ones in the latent space. Wu et al. [37] refer to the method of VAE to achieve multimodal outputs. Cycle4Completion [34] designs two cycle transformations to establish the geometric correspondence between incomplete and complete shapes in both directions. ShapeInversion [48] incorporates a well-trained GAN as an effective prior for shape completion.

Compared with the above-mentioned unpaired methods, our MFM-Net applies multi-stage matching, making the feature alignment more sufficient in the advanced stage. Besides, the shape details are enhanced in the refinement process.

3. Method

3.1. Overview

Fig. 1 shows the overall framework of our method. X_{in} and Y_{in} denote the incomplete point cloud and complete point cloud, respectively. Note that Y_{in} does not need to be the ground truth corresponding to X_{in} in unpaired task. We feed X_{in} in the completion path which outputs the completed point cloud X_f , and Y_{in} in the reconstruction path which outputs the reconstructed point cloud Y_f . The reconstructed Y_f should be as close as possible to Y_{in} . Our network is composed of feature extraction module, multi-stage feature matching module and a refinement module. Feature extraction module is responsible for extracting the global features F_x and F_y from the input point cloud X_{in} and Y_{in} . Multi-stage Feature Matching module (MFM) is designed with multi-stage process for matching the latent feature in both complete and incomplete space, and then reconstructing the coarse complete point clouds X_c and Y_c from the matched latent features. Refinement module includes three parts as its inputs to retain the local details of the input point cloud through the skip connection and avoid global shape distortion.

We follow an auto-encoder scheme in the reconstruction path and reconstruct the complete shape, while the completion path has a similar structure as the reconstruction path. Both the two paths share weights for their feature extraction module and refinement.

3.2. Feature Extraction Module

For both incomplete and complete shape X_{in} and Y_{in} , we leverage the same encoder architecture to get their global representations. Given a point set $P \in R^{N \times 3}$, our encoder extract a k-dimensional global feature $F \in R^k$. Similar to PCN [45], the encoder consists of MLP for point-wise feature extraction and finally performs maxpooling operation to obtain the global feature.

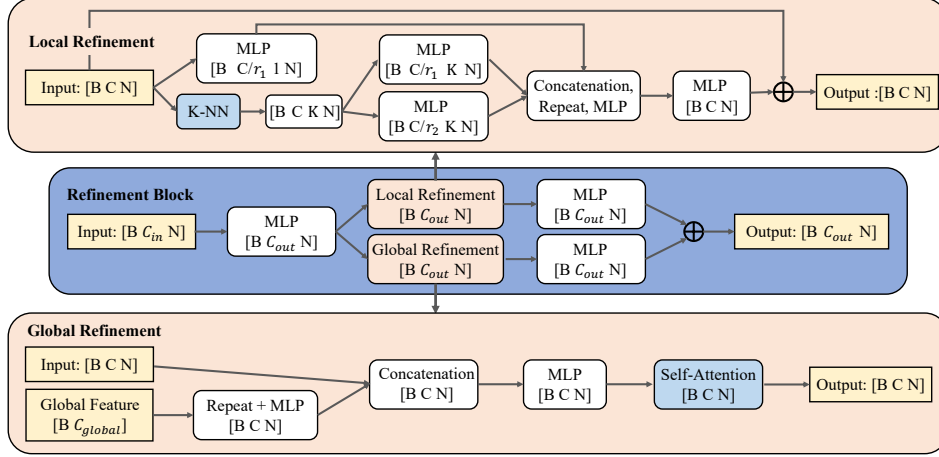


Figure 2. An illustration of our refinement block, which considers both local and global refinements.

3.3. Multi-Stage Feature Matching Module

Unlike previous methods [4, 34] that only match the global feature, we assume that the features in the advanced stage should be similar as much as possible. To this end, we propose a multi-stage matching strategy to further align the features in different stages, which can more sufficiently explore the feature correspondences.

More specifically, our MFM module involves several matching stages. For instance, we show the i -th stage matching layers in Fig. 1. The feature F_y^i in the reconstruction path passes through an MLP to get F_y^{i+1} . Since the shared-encoder could capture similar geometric primitive features across the complete and incomplete shape domain, the incomplete shape features are not far from those of the corresponding complete one (shown in Fig. 8). For this reason, for the feature F_x^i in the completion path, we apply an additional Correction Module after the MLP to explicitly find the correspondence between the complete and incomplete shape, in which we use two simple but effective fully connected layers to calculate the residual over the two domains. To better realize the matching task, we adopt the adversarial framework to make the corrected features in the completion path closer to those in the reconstruction path in each stage.

To recover the coarse shapes X_c and Y_c from the feature after multi-stage matching, we apply the same operations as PCN [45] including reshaping and folding. Finally, the global feature F is mapped to a coarse point cloud, i.e., $R^k \rightarrow R^{N \times 3}$.

3.4. Refinement Module

After obtaining two coarse outputs X_c and Y_c , our purpose is to make full use of the local patterns in input to enhance shape details, and consider the global semantic information to keep the surface smooth. The refinement block

is shown in Fig. 2, we take both local and global refinement into consideration, which can enhance the output details and avoid global shape distortion. The local refinement unit follows the work of [21], which focuses on extracting structural relations, and the global refinement unit aims to refine coarse output by considering the overall shape structure.

In the global refinement unit, we take the point-wise feature and the global feature as inputs. After repeating the global feature and passing it through an MLP, we concatenate the point-wise feature and global feature, and get the final output through another MLP and a self-attention module from [47].

As shown in Fig. 3, refinement block is used as a building block for refinement. We use hierarchy and skip connection to maintain details, which is similar to U-Net [26], and we adopt Edge-preserved Pooling (EP) module for upsampling and Edge-preserved Unpooling (EU) module for downsampling [20–22].

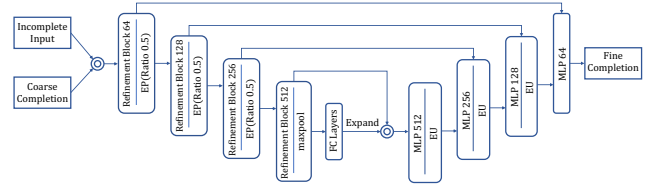


Figure 3. An illustration of our refinement framework.

3.5. Loss Function

The loss function consists of four parts: reconstruction loss, completion loss, adversarial loss and refinement loss. *Reconstruction loss*. There are two permutation-invariant metrics to compare unordered point cloud, Earth Mover’s Distance (EMD) and Chamfer Distance (CD). The EMD is

shown below.

$$\mathcal{L}_{EMD}(P, Q) = \min_{\phi: P \rightarrow Q} \frac{1}{N} \sum_{x \in P} \|x - \phi(x)\|_2 \quad (1)$$

where $P, Q \in R^{N \times 3}$ are point sets with N points, ϕ is a bijection from P to Q and $\|\dots\|_2$ means the 2-Norm of a vector. The CD is defined as:

$$\mathcal{L}_{CD}(P, Q) = \frac{1}{N_P} \sum_{p \in P} \min_{q \in Q} \|p - q\|_2^2 + \frac{1}{N_Q} \sum_{q \in Q} \min_{p \in P} \|p - q\|_2^2 \quad (2)$$

In the reconstruction path, we select EMD better to preserve the details of the reconstructed point cloud, so the loss is expressed as Eq. (3).

$$\mathcal{L}_{recon} = \mathcal{L}_{EMD}(Y_{in}, Y_c) \quad (3)$$

Completion loss. In the completion path, the incomplete shape does not have a corresponding ground truth. Therefore, in order to prevent the mode collapse and preserve the input information, we apply Unidirectional Chamfer Distance(UCD) as Eq. (4).

$$\mathcal{L}_{UCD}(P, Q) = \frac{1}{N_P} \sum_{p \in P} \min_{q \in Q} \|p - q\|_2^2 \quad (4)$$

So the loss of the completion path is expressed as:

$$\mathcal{L}_{com} = \mathcal{L}_{UCD}(X_{in}, X_c) \quad (5)$$

Adversarial loss. This loss aims to make the incomplete shape domain close to the complete shape domain. Therefore, we adopt an additional discriminator D_i to distinguish the feature F_y^i and F_x^i of i -th stage in the MFM module from *True* or *False*. Each discriminator consists of an MLP of size [1024,512,1]. For training stabilization, we perform spectral normalization [19] for each discriminator. The loss of the discriminator is defined in Eq. (6).

$$\mathcal{L}_D = \frac{1}{2k} \sum_{i=1}^k \{ \mathbb{E}_x [D_i(F_x^i)]^2 + \mathbb{E}_y [D_i(F_y^i) - 1]^2 \} \quad (6)$$

where \mathbb{E} donates the mathematical expectation, F_x^i represents the feature of the completion path at the i -th layer of the MFM module, F_y^i is the feature of the reconstruction path at the i -th layer of the MFM module and k is the number of layers of the MFM module.

Meanwhile, the loss of feature matching between the two domains can be defined as:

$$\mathcal{L}_{match} = \frac{1}{k} \sum_{i=1}^k \mathbb{E}_x [D_i(F_x^i) - 1]^2 \quad (7)$$

Refinement loss. We choose the same type of loss to train the refinement, so the loss of refinement is as Eq. (8).

$$\mathcal{L}_{refine} = \mathcal{L}_{UCD}(X_{in}, X_f) + \mathcal{L}_{CD}(Y_{in}, Y_f) \quad (8)$$

3.6. Training Strategy

We use FE , MFM and RM to represent the feature extraction module, multi-stage feature matching module and refinement respectively. In particular, we use MFM_X to represent the Correction Modules in the MFM module and let MFM_Y denote the remaining structure, and then we have $MFM = MFM_X \cup MFM_Y$. In our model, there are four types of loss functions. We use θ_D to represent the trainable parameters in $\{D_i | i = 1, \dots, k\}$, θ_{recon} to stand for the trainable parameters in $\{FE, MFM_Y\}$, θ_{com} to stand for the trainable parameters in $\{FE, MFM_X\}$ and θ_{refine} to denote the trainable parameters in $\{RM\}$.

For a given learning rate γ , we first update θ_D of all the discriminators and freeze all other parts, where the gradient optimization step is expressed as:

$$\theta_D \leftarrow \theta_D - 2\gamma \frac{\partial \mathcal{L}_D}{\partial \theta_D} \quad (9)$$

Then we use \mathcal{L}_{recon} to regularize the reconstruction path. The gradient descent step is as shown below.

$$\theta_{recon} \leftarrow \theta_{recon} - \gamma \frac{\partial \mathcal{L}_{recon}}{\partial \theta_{recon}} \quad (10)$$

To prevent the reconstruction path from being affected by the completion path, \mathcal{L}_{com} and \mathcal{L}_{match} are only adopted to update θ_{com} .

$$\theta_{com} \leftarrow \theta_{com} - \gamma [\lambda_g \frac{\partial \mathcal{L}_{match}}{\partial \theta_{com}} + \lambda_p \frac{\partial \mathcal{L}_{com}}{\partial \theta_{com}}] \quad (11)$$

where λ_g and λ_p are hyper-parameters and we set $\lambda_g = 0.1$ and $\lambda_p = 1$.

Note that we train the refinement module after some epochs until the network gets a plausible coarse result. Meanwhile, we freeze the parameters of the feature extraction module and the MFM module while training the refinement in order to protect the coarse outputs of the two different paths from being affected. Thus, the training of refinement is as follows.

$$\theta_{refine} \leftarrow \theta_{refine} - \gamma \frac{\partial \mathcal{L}_{refine}}{\partial \theta_{refine}} \quad (12)$$

4. Experiments

4.1. Evaluation on 3D-EPN Dataset

To make a fair comparison with the previous unpaired shape completion methods (i.e., Pcl2Pcl [4] and Cycle4Completion [34]), we use 3D-EPN dataset [5] with the same training and testing split for evaluation. Note that the incomplete shapes and the complete shapes do not correspond in each batch.

The quantitative results are shown in Tab. 1, we use Chamfer Distance(CD) as the evaluation metric. The experimental results show that our method is much better than

those unpaired shape completion methods in all categories and comparable with various paired methods. The visual comparison with other unpaired shape completion methods is shown in Fig. 4.

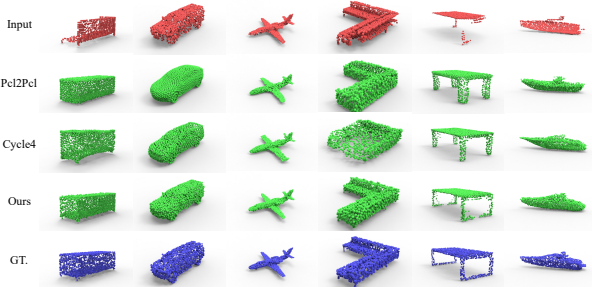


Figure 4. Visual comparison with the state-of-the-art unpaired shape completion methods on 3D-EPN dataset.

4.2. Evaluation on CRN Dataset

To verify the effectiveness of our network on different datasets and make a fair comparison with ShapeInversion [48], we also conducted an evaluation on CRN datasets [32]. The quantitative results are shown in Tab. 2. It can be seen that our model outperforms the previous unpaired methods (i.e., Pcl2Pcl [4] and ShapeInversion [32]) with a large margin in all the classes, which proves the superiority of our method. The visual comparison with other unpaired shape completion methods is shown in Fig. 5.



Figure 5. Visual comparison with the state-of-the-art unpaired shape completion methods on CRN dataset.

4.3. Evaluation on Real-World Scans

We further evaluate our network on real-world data extracted from MatterPort3D, ScanNet and KITTI. Our network trained on CRN dataset [32] can be tested directly on these real datasets without further fine-tuning process. We quantitatively evaluate our results with Unidirectional Chamfer Distance (UCD) and Unidirectional Haus-

dorff Distance (UHD) with quantitative and qualitative results shown in Tab. 3 and Fig. 6, respectively. UHD can be defined as:

$$\mathcal{L}_{UHD}(P, Q) = \max_{p \in P} \min_{q \in Q} \|p - q\|_2^2 \quad (13)$$

Table 3. Shape completion results on the real scans. The numbers shown are $[UCD/UHD]$ (lower is better), where UCD is scaled by 10^4 and UHD is scaled by 10^2 .

Methods	ScanNet		MatterPort3D		KITTI
	Chair	Table	Chair	Table	Car
Pcl2Pcl	17.3/10.1	9.1/11.8	15.9/10.5	6.0/11.8	9.2/14.1
ShapeInversion	3.2/10.1	3.3/11.9	3.6/10.0	3.1/11.8	2.9/13.8
Ours Coarse	4.8/6.4	4.0/6.3	5.2/8.4	7.1/10.0	4.9/6.0
Ours Refine	1.1/1.9	0.9/1.6	1.0/ 1.9	0.8/1.7	0.3/1.1

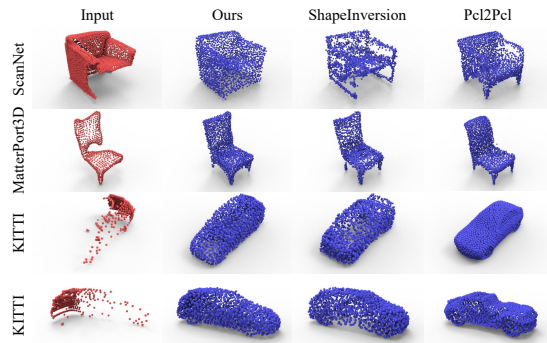


Figure 6. Shape completion on real-world partial scans.

4.4. Analysis of Refinement

As we have claimed that the refinement module in our network can enhance the details of the coarse output, we evaluate our network both with and without the refinement and the results are shown in Tab. 1 and Tab. 2. It can be observed that the refinement module can boost the completion performance. Also, we visualize some intermediate results of our network in Fig. 7. We can see the refined results in the third column have more details with a smooth surface.

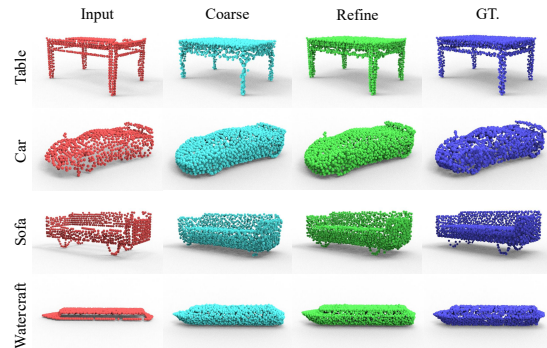


Figure 7. Visualization of coarse and refine outputs.

Table 1. Shape completion results on 3D-EPN dataset. The numbers shown are CD (lower is better), which is scaled by 10^4 . MFM-Net outperforms other unpaired methods by a large margin, and is comparable to the various paired methods.

	Methods	Average	Plane	Cabinet	Car	Chair	Lamp	Sofa	Table	Boat
<i>paired</i>	3D-EPN [5]	29.1	60.0	27.0	24.0	16.0	38.0	45.0	14.0	9.0
	FoldingNet [43]	9.2	2.4	8.5	7.2	10.3	14.1	9.1	13.6	8.8
	PCN [45]	7.6	2.0	8.0	5.0	9.0	13.0	8.0	10.0	6.0
	TopNet [28]	8.4	2.5	8.8	5.9	9.3	12.0	8.4	13.5	7.1
	SA-Net [35]	7.7	2.2	9.1	5.6	8.9	10.0	7.8	9.9	7.2
<i>unpaired</i>	AE(baseline) [4]	25.4	4.0	37.0	19.0	31.0	26.0	30.0	44.0	12.0
	Pcl2Pcl [4]	17.4	4.0	19.0	10.0	20.0	23.0	26.0	26.0	11.0
	Cycle4Completion [34]	14.3	3.7	12.6	8.1	14.6	18.2	26.2	22.5	8.7
	Ours Coarse	10.0	2.6	10.9	6.3	12.4	15.1	10.5	15.8	6.5
	Ours Refine	9.0	2.1	10.8	6.0	11.1	12.7	9.3	14.5	5.2

Table 2. Shape completion results on CRN dataset. The numbers shown are CD (lower is better), which is scaled by 10^4 . MFM-Net outperforms other unpaired methods by a large margin, and is comparable to the various paired methods.

	Methods	Average	Plane	Cabinet	Car	Chair	Lamp	Sofa	Table	Boat
<i>paired</i>	PCN [45]	9.1	3.5	11.3	6.4	11.0	11.6	11.5	10.4	7.4
	TopNet [28]	11.4	4.1	12.9	7.8	13.4	14.8	16.0	12.9	8.9
	MSN [17]	8.8	2.9	12.5	7.1	10.6	9.3	12.0	9.6	6.5
	CRN [32]	8.0	2.3	11.4	6.2	8.8	8.5	11.3	9.3	6.1
<i>unpaired</i>	Pcl2Pcl [4]	22.4	9.8	27.1	15.8	26.9	25.7	34.1	23.6	15.7
	ShapeInversion [48]	14.9	5.6	16.1	13.0	15.4	18.0	24.6	16.2	10.1
	Ours Coarse	11.6	3.8	12.4	9.0	13.9	14.1	18.9	11.7	8.7
	Ours Refine	10.3	3.2	11.5	8.7	12.2	11.7	17.6	10.2	7.3

4.5. Analysis of Different Training Strategies

In our model, the completion loss \mathcal{L}_{com} and the adversarial loss \mathcal{L}_{match} are used to update θ_{com} only. However, \mathcal{L}_{com} and \mathcal{L}_{match} involve not only the Correction Modules but also the remaining part of the MFM module. To evaluate the effectiveness of other potential training strategies, similar to Sec. 3.6, we use θ_{all} to denote the trainable parameters in $\{FE, MFM\}$. Then we develop the variations of (a) $\partial\mathcal{L}_{com}/\partial\theta_{all}$ and (b) $\partial\mathcal{L}_{match}/\partial\theta_{all}$ to replace $\partial\mathcal{L}_{com}/\partial\theta_{com}$ or $\partial\mathcal{L}_{match}/\partial\theta_{com}$ in Eq. (11).

The results are reported in Tab. 4. We observed awful results in (a) and (b) because the reconstruction path is affected by the completion path, which leads to a failure to reconstruct the complete shape input Y_{in} .

Table 4. Results of different training strategies ($CD \times 10^4$).

Methods	Average	Car	Chair	Lamp	Sofa	Table
$\partial\mathcal{L}_{com}/\partial\theta_{all}$	22.9	9.8	22.3	27.3	30.1	25.0
$\partial\mathcal{L}_{match}/\partial\theta_{all}$	21.7	10.5	22.0	26.1	32.3	17.5
Original Model	13.5	9.0	13.9	14.1	18.9	11.7

4.6. Visual analysis of latent feature distribution

In Fig. 8, we use t-SNE [29] to visualize the features in the high-dimensional latent space as 2D points. The distance of points can reflect the similarity of the corresponding latent features to a certain extent. The red dots represent the global features from complete shapes and the blue dots represent the global features from the incomplete shapes before MFM module. The green dots represent the transferred global features of the incomplete shape after MFM module.

As shown in Fig. 8a, the features before MFM module of the two paths are not exactly the same indicating that the correspondences in the incomplete shape and the complete shape can not be fully explored. As shown in Fig. 8b, the global features after MFM could be similar enough to adapt to the task of point cloud completion. We also visualize the features of Pcl2Pcl [4] on the same instances, as shown in Fig. 8c and Fig. 8d. Pcl2Pcl tends to output a reasonable complete shape without paying attention to maintaining the information of the incomplete shape input, resulting in the fact that its transformed features are still far away from those of the corresponding ground truth. Furthermore, we choose two labels (i.e., 4 and 5) and visualize the shape represented by these points, including the incomplete in-

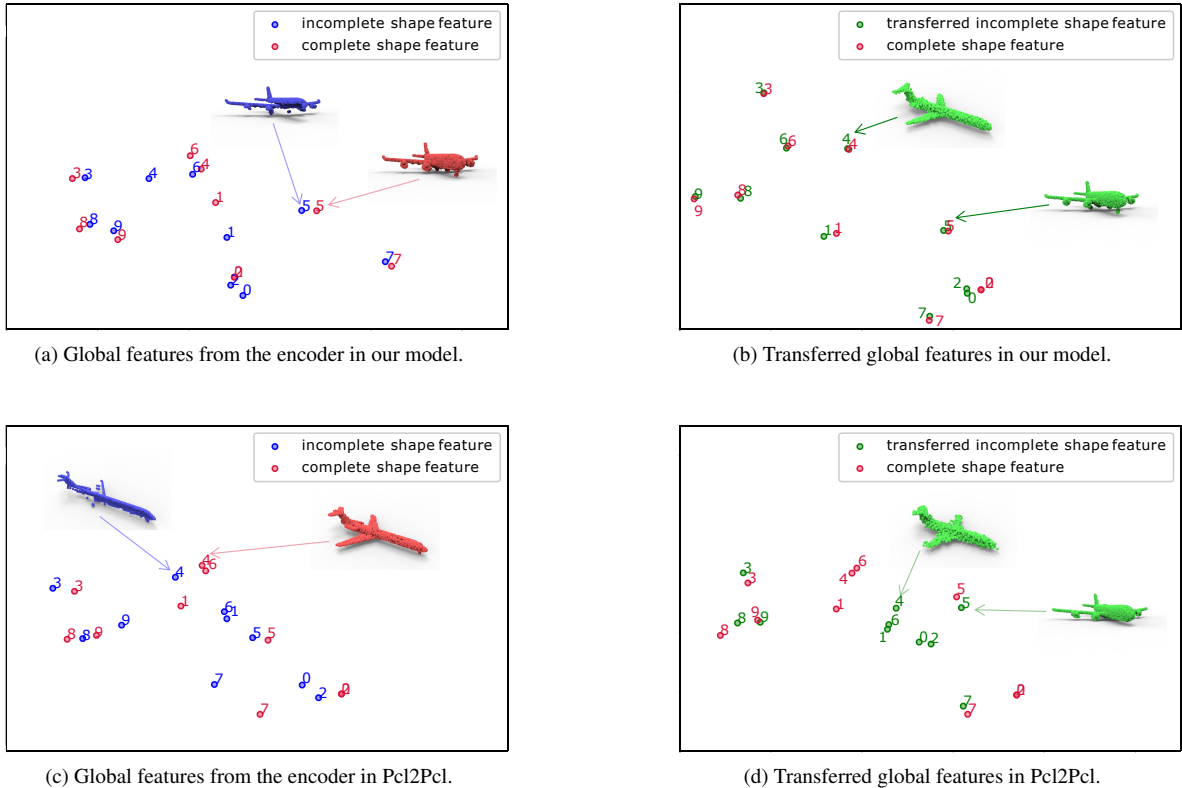


Figure 8. Visualization of latent space. (a) and (b) show the results of our model, (c) and (d) show the results of Pcl2Pcl. We further select two labels (i.e., 4 and 5) to visualize the shape that these points represent. These pictures can show that our network can effectively match features, while Pcl2Pcl can't do.

puts, ground truths and coarse completed shapes.

4.7. More Analysis

In this chapter, we will further analyze each part of our network with results shown in Tab. 5. We perform this evaluation on five categories in CRN dataset [32].

Correction Module Evaluation. To evaluate the effectiveness of the major components in our framework, we give a study about removing the Correction Module and remaining only one path in the decoder. In this case, we retrained the network for evaluation and the results are shown as *w/o Correction Module* in Tab. 5. The network performance decreases without Correction Module, showing the effectiveness of Correction Module.

Comparison with matching the global feature only. In order to explore the performance of our model that only matches the global features before MFM module between incomplete and complete shapes, we evaluate MFM-Net under this circumstance. The result is shown as *Only Global Feature* in Tab. 5.

Comparison with using two separated encoders. In order to analyze the necessity of encoder parameter sharing, we adopted two separated encoders and retrained our network.

The result is shown as *Separate Encoders* in Tab. 5.

Table 5. More Analysis ($CD \times 10^4$).

Methods	Average	Car	Chair	Lamp	Sofa	Table
w/o Correction Module	19.7	10.9	20.4	19.1	30.5	17.6
Only Global Feature	19.6	10.4	18.0	17.3	39.8	12.5
Separate Encoders	16.2	10.7	16.5	19.7	19.5	14.4
Original Model	13.5	9.0	13.9	14.1	18.9	11.7

5. Conclusions

We propose the MFM-Net for unpaired point cloud completion task. Different from existing approaches that only match the global features, our model introduces a dual-path framework and successfully establishes a multi-stage matching relationship between incomplete and complete shapes, enhancing the understanding of the complete and incomplete shape correspondence. We also apply a refinement module that considers both local and global refinements to retain the local details. Furthermore, our model is evaluated on several widely used datasets, achieving state-of-the-art performance by a large margin compared with other unpaired completion methods. As our approach still needs unpaired supervision, we plan to explore the completion task in a fully unsupervised manner as future work.

References

- [1] Antonio Alliegro, Diego Valsesia, Giulia Fracastoro, Enrico Magli, and Tatiana Tommasi. Denoise and contrast for category agnostic shape completion. In *Proceedings of the IEEE/CVF Conference on Computer Vision and Pattern Recognition*, pages 4629–4638, 2021. 3
- [2] Matthew Berger, Andrea Tagliasacchi, Lee Seversky, Pierre Alliez, Joshua Levine, Andrei Sharf, and Claudio Silva. State of the art in surface reconstruction from point clouds. In *Eurographics 2014-State of the Art Reports*, volume 1, pages 161–185, 2014. 3
- [3] Angel X Chang, Thomas Funkhouser, Leonidas Guibas, Pat Hanrahan, Qixing Huang, Zimo Li, Silvio Savarese, Manolis Savva, Shuran Song, Hao Su, et al. Shapenet: An information-rich 3d model repository. *arXiv preprint arXiv:1512.03012*, 2015. 1
- [4] Xuelin Chen, Baoquan Chen, and Niloy J Mitra. Unpaired point cloud completion on real scans using adversarial training. In *International Conference on Learning Representations*, 2019. 1, 2, 3, 4, 5, 6, 7
- [5] Angela Dai, Charles Ruizhongtai Qi, and Matthias Nießner. Shape completion using 3d-encoder-predictor cnns and shape synthesis. In *Proceedings of the IEEE Conference on Computer Vision and Pattern Recognition*, pages 5868–5877, 2017. 3, 5, 7
- [6] James Davis, Stephen R Marschner, Matt Garr, and Marc Levoy. Filling holes in complex surfaces using volumetric diffusion. In *Proceedings. First International Symposium on 3D Data Processing Visualization and Transmission*, pages 428–441. IEEE, 2002. 3
- [7] Pedro F Felzenszwalb, Ross B Girshick, David McAllester, and Deva Ramanan. Object detection with discriminatively trained part-based models. *IEEE transactions on pattern analysis and machine intelligence*, 32(9):1627–1645, 2009. 3
- [8] Bingchen Gong, Yinyu Nie, Yiqun Lin, Xiaoguang Han, and Yizhou Yu. Me-pcn: Point completion conditioned on mask emptiness. In *Proceedings of the IEEE/CVF International Conference on Computer Vision*, pages 12488–12497, 2021. 3
- [9] Saurabh Gupta, Pablo Arbeláez, Ross Girshick, and Jitendra Malik. Aligning 3d models to rgb-d images of cluttered scenes. In *Proceedings of the IEEE conference on computer vision and pattern recognition*, pages 4731–4740, 2015. 3
- [10] Feng Han and Song-Chun Zhu. Bottom-up/top-down image parsing with attribute grammar. *IEEE transactions on pattern analysis and machine intelligence*, 31(1):59–73, 2008. 3
- [11] Zhizhong Han, Xiyang Wang, Yu-Shen Liu, and Matthias Zwicker. Multi-angle point cloud-vae: Unsupervised feature learning for 3d point clouds from multiple angles by joint self-reconstruction and half-to-half prediction. In *2019 IEEE/CVF International Conference on Computer Vision (ICCV)*, pages 10441–10450. IEEE, 2019. 3
- [12] Wei Hu, Zeqing Fu, and Zongming Guo. Local frequency interpretation and non-local self-similarity on graph for point cloud inpainting. *IEEE Transactions on Image Processing*, 28(8):4087–4100, 2019. 3
- [13] Tianxin Huang, Hao Zou, Jinhao Cui, Xuemeng Yang, Mengmeng Wang, Xiangrui Zhao, Jiangning Zhang, Yi Yuan, Yifan Xu, and Yong Liu. Rfnet: Recurrent forward network for dense point cloud completion. In *Proceedings of the IEEE/CVF International Conference on Computer Vision*, pages 12508–12517, 2021. 3
- [14] Zitian Huang, Yikuan Yu, Jiawen Xu, Feng Ni, and Xinyi Le. Pf-net: Point fractal network for 3d point cloud completion. In *Proceedings of the IEEE/CVF Conference on Computer Vision and Pattern Recognition*, pages 7662–7670, 2020. 1, 3
- [15] Yangyan Li, Angela Dai, Leonidas Guibas, and Matthias Nießner. Database-assisted object retrieval for real-time 3d reconstruction. In *Computer graphics forum*, volume 34, pages 435–446. Wiley Online Library, 2015. 3
- [16] Ming Liu. Robotic online path planning on point cloud. *IEEE transactions on cybernetics*, 46(5):1217–1228, 2015. 1
- [17] Minghua Liu, Lu Sheng, Sheng Yang, Jing Shao, and Shi-Min Hu. Morphing and sampling network for dense point cloud completion. In *Proceedings of the AAAI conference on artificial intelligence*, volume 34, pages 11596–11603, 2020. 1, 3, 7
- [18] Niloy J Mitra, Leonidas J Guibas, and Mark Pauly. Partial and approximate symmetry detection for 3d geometry. *ACM Transactions on Graphics (TOG)*, 25(3):560–568, 2006. 3
- [19] Takeru Miyato, Toshiki Kataoka, Masanori Koyama, and Yuichi Yoshida. Spectral normalization for generative adversarial networks. *arXiv preprint arXiv:1802.05957*, 2018. 5
- [20] Liang Pan. Ecg: Edge-aware point cloud completion with graph convolution. *IEEE Robotics and Automation Letters*, 5(3):4392–4398, 2020. 4
- [21] Liang Pan, Xinyi Chen, Zhongang Cai, Junzhe Zhang, Haiyu Zhao, Shuai Yi, and Ziwei Liu. Variational relational point completion network. In *Proceedings of the IEEE/CVF Conference on Computer Vision and Pattern Recognition*, pages 8524–8533, 2021. 1, 3, 4
- [22] Liang Pan, Chee-Meng Chew, and Gim Hee Lee. Pointatrousgraph: Deep hierarchical encoder-decoder with point atrous convolution for unorganized 3d points. In *2020 IEEE International Conference on Robotics and Automation (ICRA)*, pages 1113–1120. IEEE, 2020. 4
- [23] Charles R Qi, Hao Su, Kaichun Mo, and Leonidas J Guibas. Pointnet: Deep learning on point sets for 3d classification and segmentation. In *Proceedings of the IEEE conference on computer vision and pattern recognition*, pages 652–660, 2017. 1, 3
- [24] Tahir Rabbani, Frank Van Den Heuvel, and George Vosselmann. Segmentation of point clouds using smoothness constraint. *International archives of photogrammetry, remote sensing and spatial information sciences*, 36(5):248–253, 2006. 1
- [25] Audrey Richard, Ian Cherabier, Martin R Oswald, Marc Pollefeys, and Konrad Schindler. Kaplan: A 3d

- point descriptor for shape completion. *arXiv preprint arXiv:2008.00096*, 2020. 3
- [26] Olaf Ronneberger, Philipp Fischer, and Thomas Brox. U-net: Convolutional networks for biomedical image segmentation. In *International Conference on Medical image computing and computer-assisted intervention*, pages 234–241. Springer, 2015. 4
- [27] David Stutz and Andreas Geiger. Learning 3d shape completion from laser scan data with weak supervision. In *Proceedings of the IEEE Conference on Computer Vision and Pattern Recognition*, pages 1955–1964, 2018. 3
- [28] Lyne P Tchammi, Vineet Kosaraju, Hamid Rezatofighi, Ian Reid, and Silvio Savarese. Topnet: Structural point cloud decoder. In *Proceedings of the IEEE/CVF Conference on Computer Vision and Pattern Recognition*, pages 383–392, 2019. 7
- [29] Laurens Van der Maaten and Geoffrey Hinton. Visualizing data using t-sne. *Journal of machine learning research*, 9(11), 2008. 7
- [30] Weiyue Wang, Qiangui Huang, Suya You, Chao Yang, and Ulrich Neumann. Shape inpainting using 3d generative adversarial network and recurrent convolutional networks. In *Proceedings of the IEEE international conference on computer vision*, pages 2298–2306, 2017. 3
- [31] Xiaogang Wang, Marcelo H Ang, and Gim Hee Lee. Voxel-based network for shape completion by leveraging edge generation. In *Proceedings of the IEEE/CVF International Conference on Computer Vision*, pages 13189–13198, 2021. 3
- [32] Xiaogang Wang, Marcelo H Ang Jr, and Gim Hee Lee. Cascaded refinement network for point cloud completion. In *Proceedings of the IEEE/CVF Conference on Computer Vision and Pattern Recognition*, pages 790–799, 2020. 6, 7, 8
- [33] Yue Wang and Justin M Solomon. Deep closest point: Learning representations for point cloud registration. In *Proceedings of the IEEE/CVF International Conference on Computer Vision*, pages 3523–3532, 2019. 1
- [34] Xin Wen, Zhizhong Han, Yan-Pei Cao, Pengfei Wan, Wen Zheng, and Yu-Shen Liu. Cycle4completion: Unpaired point cloud completion using cycle transformation with missing region coding. In *Proceedings of the IEEE/CVF Conference on Computer Vision and Pattern Recognition*, pages 13080–13089, 2021. 1, 2, 3, 4, 5, 7
- [35] Xin Wen, Tianyang Li, Zhizhong Han, and Yu-Shen Liu. Point cloud completion by skip-attention network with hierarchical folding. In *Proceedings of the IEEE/CVF Conference on Computer Vision and Pattern Recognition*, pages 1939–1948, 2020. 3, 7
- [36] Xin Wen, Peng Xiang, Zhizhong Han, Yan-Pei Cao, Pengfei Wan, Wen Zheng, and Yu-Shen Liu. Pmp-net: Point cloud completion by learning multi-step point moving paths. In *Proceedings of the IEEE/CVF Conference on Computer Vision and Pattern Recognition*, pages 7443–7452, 2021. 3
- [37] Rundi Wu, Xuelin Chen, Yixin Zhuang, and Baoquan Chen. Multimodal shape completion via conditional generative adversarial networks. In *Computer Vision—ECCV 2020: 16th European Conference, Glasgow, UK, August 23–28, 2020, Proceedings, Part IV 16*, pages 281–296. Springer, 2020. 3
- [38] Yaqi Xia, Yan Xia, Wei Li, Rui Song, Kailang Cao, and Uwe Stilla. Asfm-net: Asymmetrical siamese feature matching network for point completion. *arXiv preprint arXiv:2104.09587*, 2021. 3
- [39] Peng Xiang, Xin Wen, Yu-Shen Liu, Yan-Pei Cao, Pengfei Wan, Wen Zheng, and Zhizhong Han. Snowflakenet: Point cloud completion by snowflake point deconvolution with skip-transformer. In *Proceedings of the IEEE/CVF International Conference on Computer Vision*, pages 5499–5509, 2021. 3
- [40] Chulin Xie, Chuxin Wang, Bo Zhang, Hao Yang, Dong Chen, and Fang Wen. Style-based point generator with adversarial rendering for point cloud completion. In *Proceedings of the IEEE/CVF Conference on Computer Vision and Pattern Recognition*, pages 4619–4628, 2021. 3
- [41] Haozhe Xie, Hongxun Yao, Shangchen Zhou, Jiageng Mao, Shengping Zhang, and Wenxiu Sun. Grnet: Gridding residual network for dense point cloud completion. In *European Conference on Computer Vision*, pages 365–381. Springer, 2020. 1, 3
- [42] Bo Yang, Hongkai Wen, Sen Wang, Ronald Clark, Andrew Markham, and Niki Trigoni. 3d object reconstruction from a single depth view with adversarial learning. In *Proceedings of the IEEE International Conference on Computer Vision Workshops*, pages 679–688, 2017. 3
- [43] Yaoqing Yang, Chen Feng, Yiru Shen, and Dong Tian. Foldingnet: Point cloud auto-encoder via deep grid deformation. In *Proceedings of the IEEE Conference on Computer Vision and Pattern Recognition*, pages 206–215, 2018. 7
- [44] Xumin Yu, Yongming Rao, Ziyi Wang, Zuyan Liu, Jiwen Lu, and Jie Zhou. Pointnet: Diverse point cloud completion with geometry-aware transformers. In *Proceedings of the IEEE/CVF International Conference on Computer Vision*, pages 12498–12507, 2021. 3
- [45] Wentao Yuan, Tejas Khot, David Held, Christoph Mertz, and Martial Hebert. Pcn: Point completion network. In *2018 International Conference on 3D Vision (3DV)*, pages 728–737. IEEE, 2018. 1, 3, 4, 7
- [46] Xiangyu Yue, Bichen Wu, Sanjit A Seshia, Kurt Keutzer, and Alberto L Sangiovanni-Vincentelli. A lidar point cloud generator: from a virtual world to autonomous driving. In *Proceedings of the 2018 ACM on International Conference on Multimedia Retrieval*, pages 458–464, 2018. 1
- [47] Han Zhang, Ian Goodfellow, Dimitris Metaxas, and Augustus Odena. Self-attention generative adversarial networks. In *International conference on machine learning*, pages 7354–7363. PMLR, 2019. 4
- [48] Junzhe Zhang, Xinyi Chen, Zhongang Cai, Liang Pan, Haiyu Zhao, Shuai Yi, Chai Kiat Yeo, Bo Dai, and Chen Change Loy. Unsupervised 3d shape completion through gan inversion. In *Proceedings of the IEEE/CVF Conference on Computer Vision and Pattern Recognition*, pages 1768–1777, 2021. 3, 6, 7
- [49] Wenxiao Zhang, Qingan Yan, and Chunxia Xiao. Detail preserved point cloud completion via separated feature aggregation. In *Computer Vision—ECCV 2020: 16th European Conference, Glasgow, UK, August 23–28, 2020, Proceedings, Part XXV 16*, pages 512–528. Springer, 2020. 3

- [50] Yanan Zhang, Di Huang, and Yunhong Wang. Pc-rgnn: Point cloud completion and graph neural network for 3d object detection. In *Proceedings of the AAAI Conference on Artificial Intelligence*, volume 35, pages 3430–3437, 2021. [3](#)